J Solid State Electrochem (2009) 13:671–677
DOI 10.1007/s10008-008-0594-3

ORIGINAL PAPER

Electrochemical studies on Zn deposition and dissolution in sulphate electrolyte

Tzvetanka Boiadjieva · Milko Monev · Alexander Tomandl · Hermann Kronberger · Günter Fafilek

Received: 14 April 2008 / Accepted: 19 May 2008 / Published online: 13 June 2008

Abstract The electrochemical deposition and dissolution of Zn on Pt electrode in sulphate electrolyte was investigated by electrochemical methods in an attempt to contribute to the better understanding of the more complex Zn–Cr alloy electrodeposition process. A decrease of the Zn electrolyte pH (from 5.4 to 1.0) so as to minimise/avoid the formation of hydroxo-products of Cr in the electrolyte for deposition of alloy coatings decreases the current efficiency for the Zn reaction, but the rate of the cathode reaction increases significantly due to intense hydrogen evolution. The results of the investigations in Zn electrolytes with pH 1.0–1.6 indicate that Zn bulk deposition is preceded by hydrogen evolution, stepwise Zn underpotential deposition (UPD) and formation of a Zn–Pt alloy. Hydrogen evolution from H_2O starts in the potential range of Zn bulk deposition. Data obtained from the electrochemical quartz crystal microbalance (EQCM) measurements support the assumption that electrochemical deposition of Zn proceeds at potentials more positive than the reversible potential of Zn. Anodic potentiodynamic curves for galvanostatically and potentiostatically deposited Zn layers provide indirect evidence about the dissolution of Zn from an alloy with the Pt substrate. The presumed potential of co-deposition of Cr (−1.9 V vs. Hg/Hg_2SO_4) is reached at a current density of about 300 mA cm^{-2}.

T. Boiadjieva
Center of Competence in Applied Electrochemistry GmbH,
Viktor Kaplan Strasse 2,
2700 Wiener Neustadt, Austria

M. Monev (✉)
Institute of Physical Chemistry, Bulg. Acad. Sci.,
1113 Sofia, Bulgaria
e-mail: monev@ipc.bas.bg

A. Tomandl
voestalpine Stahl GmbH,
Voestalpine-Strasse 3,
4020 Linz, Austria

H. Kronberger · G. Fafilek
TU-Vienna, Institute for Chemical Technology and Analytics,
Getreidemarkt 9/164ec,
A-1060 Vienna, Austria

Introduction

The electrochemical deposition of Zn still attracts much attention [1–16]. Most of the studies on Zn deposition are related to Zn alloy electrodeposition [8, 10, 14–17]. The iron group metal alloys with Zn have been investigated most actively as a result of the frantic research by steel manufacturers to develop highly corrosion-resistant alloy-plated steel sheet for automotive body panels [1]. Zn–Fe, Zn–Co and Zn–Ni alloys have significantly higher corrosion resistance in comparison to that of pure Zn coatings. On the other hand, the anomalous co-deposition of the iron group metals (Fe, Co, Ni) with Zn is of academic interest. Different aspects such as the effect of the substrate [4–8, 10], the anion adsorption strength [2, 3], the presence of ions of an alloying element [10, 14], the different organic additives [4, 5, 9, 11–13], etc. on the initial stages and on bulk Zn deposition have been investigated. Calculations and experimental determinations of some electrochemical parameters for Zn/Zn(II) on different electrodes are presented [2, 3, 8, 9, 16]. Electrodeposition of Zn onto Pt [2, 3, 7, 18–21], Au [2, 15, 18, 22], Cu [22], Fe [11, 12, 14, 23], Pd [19], Ni [24], etc. has been found to also occur at potentials more positive than the standard Zn electrode potential. AFM analysis shows that Zn electrodeposition

onto a steel substrate begins in the underpotential deposition (UPD) region with formation of nanometric circular clusters homogeneously distributed on the steel surface [25]. UPD is an issue of both theoretical and practical interest in relation to the deposition at cathode overpotentials (OPD) [7, 21], the electrocatalysis of oxidation of organic compounds [26], the hydrogen evolution reaction (HER) [23, 27, 28], etc. The UPD of Zn onto Pt is shown to produce an electrode surface suitable for the evaluation of Zn overpotential kinetics [21]. The influence of anions and organic additives on the UPD of Zn has been studied on the assumption that the UPD of metals also plays an important role in the anomalous co-deposition of Zn alloys [10, 14]. The inhibitory effect of Zn UPD on Zn–Co alloy electrodeposition has been investigated, and the formation of different cobalt-rich alloys has been established in the potential range where Zn deposits underpotentially [10].

The present work is part of a comprehensive study on the electrochemical deposition of Zn–Cr alloy coatings [29–32] and presents results from electrochemical studies on the deposition and dissolution of Zn on Pt electrodes in acidic sulphate electrolytes.

Experimental

All chemicals used were of analytical grade. Electrolytes containing 0.6 M $ZnSO_4 \cdot 7H_2O$ with or without 0.5 M Na_2SO_4 were used for voltammetric investigation and Zn deposition experiments. pH was adjusted by addition of H_2SO_4 solution (1:1).

The effect of electrochemical conditions on Zn deposition was investigated by cyclic voltammetry using a three-electrode cell with a volume of 50 ml comprising a working polycrystalline Pt electrode with 0.16 cm^2 surface area, a Pt counter electrode and a Hg/Hg_2SO_4 reference electrode. The scanning rate was 25 mV s^{-1}. The initial potential was the open circuit potential, and the polarisation was first in the negative direction. All experiments were carried out using a potentiostat/galvanostat (EG&G Princeton Applied Research, Model 263A) and SoftCorr II software.

Electrochemical quartz crystal microbalance (EQCM) was used for investigating the electrochemical process in the potential region before the onset of bulk Zn deposition. The EQCM is a sensitive technique for measuring changes in mass, and it has been applied to analyse electrochemical and adsorption processes during Zn electrodeposition [7, 13, 15, 27]. The electrogravimetric measurements were performed with a quartz crystal microbalance (Princeton Applied Research, Model QCM922) combined with a potentiostat/galvanostat (EG&G PAR, Model 263A) and using the WinEchem Software (Princeton Applied Research). A standard 9 MHz AT-cut quartz crystal covered with a polycrystalline Pt film on both sides was used as working electrode. The geometric area of the Pt electrode was 0.2 cm^2. A Pt sheet and an Hg/Hg_2SO_4 electrode were used as counter and reference electrodes, respectively.

Zn coatings were deposited under galvanostatic and potentiostatic conditions onto Pt substrates with dimensions 2×1 cm. Pre-treatment of the electrodes included electrochemical degreasing and pickling in 10% solution of H_2SO_4. Coatings were deposited at current densities within the 5- to 300-mA cm^{-2} range, at a pH of 1.0–5.4 and a temperature of 25 °C without agitation. Platinised Ti was used as an anode.

Anodic potentiodynamic polarisation was applied to study the dissolution of the coatings after galvanostatic and potentiostatic deposition. Cathode current efficiency was determined gravimetrically. X-ray microprobe analyses (EDX) were used for Zn detection after galvanostatic and potentiostatic deposition (JCXA 733 Jeol, Japan). The morphology of the Zn coatings was observed using a scanning electron microscopy (SEM) (JSM 5300, Jeol, Japan).

Results

Zn and Zn-based (Zn–Co, Zn–Ni and Zn–Fe) alloy coatings are most often electrodeposited on steel parts from weakly acidic, sulphate and/or chloride electrolytes. The pH of these electrolytes is within the range from 4.5 to 6.0, and they cannot be used as basic electrolytes for electrodeposition of Zn–Cr alloy coatings because, at these pH values, Cr(III) hydroxide is formed [33]. According to some authors, hydroxides of Zn and Cr are formed simultaneously in electrolytes for Zn–Cr alloy deposition at a pH of about 4.0 [34, 35]. Hence, more acidic solutions should be used for the production of Zn–Cr alloy coatings. Sulphate electrolytes with a pH of 1.5–2.0 are used for high-speed Zn electrodeposition on steel strips and rods.

The voltammograms obtained in this work from zinc-containing electrolytes on Pt electrode were plotted to potentials highly negative or positive for the Zn reaction to be related with Cr reduction. According to the two-step mechanism (Cr(III)→Cr(II)→Cr(0)), reduction of Cr may proceed at potentials more negative than −1.52 V (Hg/Hg_2SO_4), whilst our preliminary studies have shown that a potential value of about −1.9 V (Hg/Hg_2SO_4) must be reached for deposition and co-deposition of Cr, which is in agreement with literature data [36–38]. Active and transpassive dissolution of Cr depend on the pH of the medium, and the transpassive region starts at potentials more positive than +0.5 V [39].

Figure 1 illustrates the effect of electrolyte pH on the shape of the voltammograms in Zn electrolyte (0.6 M

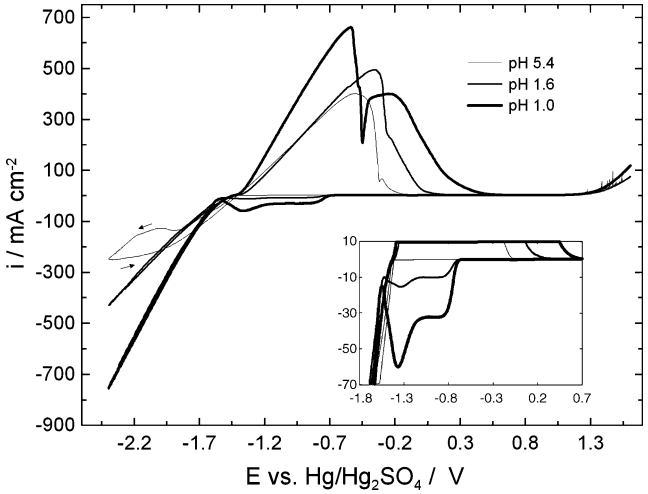

Fig. 1 Voltammograms showing the effect of electrolyte pH on the deposition and dissolution of Zn in 0.6 M $ZnSO_4$ solution. Vertex potential −2.4 V. *Inset* zoom in the potential range −1.8 to +0.7 V

$ZnSO_4$). At pH 5.4, reduction of Zn starts at about −1.4 V. No hydrogen evolution is observed up to this potential and a limiting current density for the Zn reaction is reached (120 mA cm^{-2}) leading to superficial roughening of the coating. As a result, the current density (which includes also the HER) in the backward scan is higher and a cathode loop is observed. With the decrease of the solution pH, visible hydrogen evolution starts at about −0.7 V, and this is the potential region where the course of the voltammogram changes.

For comparison, Fig. 2 presents the polarisation curves of hydrogen evolution on Pt electrode in 0.5 M Na_2SO_4 solution at the same pH values. Evolution of hydrogen starts at potentials close to those measured for the Zn electrolyte. A limiting current density is observed in the more acidic solutions, too. At sufficiently negative potentials, hydrogen evolution from water starts ($2H_2O+2e^-\rightarrow H_2\uparrow+2OH^-$) and the current increases.

With decrease of electrolyte pH, the rate of the overall cathode reaction increases (Fig. 1). An increase in area of the anodic peak for Zn is also observed, but on the other hand, the current efficiency of the Zn reaction decreases (from 98% at pH 5.4 to 88% at pH 1.0 for 100 mA cm^{-2} current density), i.e. the contribution of the hydrogen evolution reaction to the overall cathode reaction increases. An interesting feature of the curve at pH 1.0 is the splitting of the peak of Zn dissolution. Such an effect is observed in several cases: on potentiodynamic dissolution of coatings electrodeposited at high current densities, respectively, highly negative potentials or on prolonged electrodeposition. The peak splitting is not related to a particular anodic potential. All the above cases share in common the formation of a deposit phase and superficial roughening of the coatings during the cathode process. On slower dissolution, i.e. at lower scan rate or when the solution is agitated, the above effect disappears, which is an indication that the peak splitting is affected by diffusion limitations during the dissolution of Zn. In the potential region of anodic peak splitting, hydrogen bubbles can be seen on the surface of the coating, which most probably were incorporated into the coarse structure of the coating at the highly negative potentials. With the increase of the scan rate and of the stirring intensity, the cathode current increases, proving that the HER up to Zn OPD and the bulk reduction of Zn are also dominated by mass transfer effects [9, 12], whilst the onset of Zn electrodeposition is not affected.

Besides the decline in the current efficiency for the Zn reaction, the decrease in electrolyte pH also leads to a significant increase of the current density for reaching the

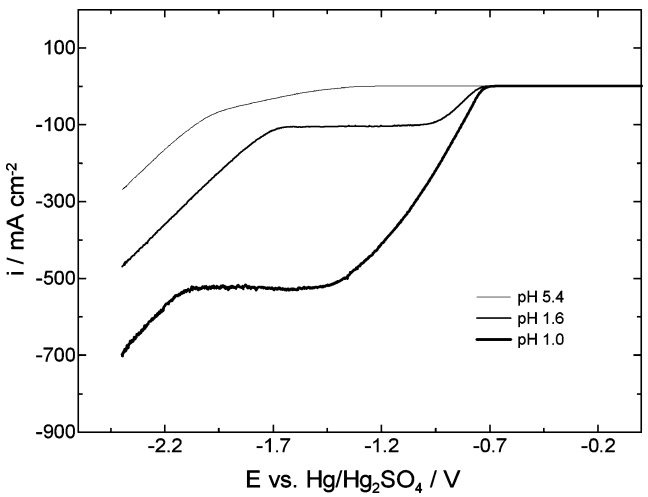

Fig. 2 Cathode voltammetric curves obtained for Pt in 0.5 M Na_2SO_4 solution at different pH values. Vertex potential −2.4 V

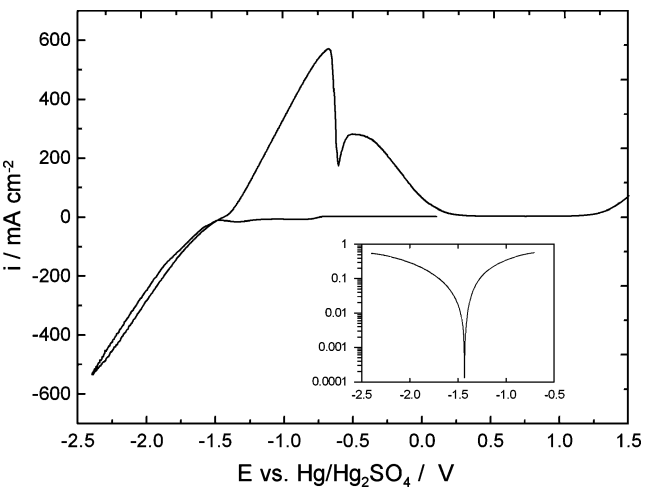

Fig. 3 Voltammogram in 0.6 M $ZnSO_4$+0.5 M Na_2SO_4 solution, pH 1.6. Vertex potential −2.4 V. *Inset* semi-logarithmic representation of the voltammogram in the potential range of cathode/anode transition

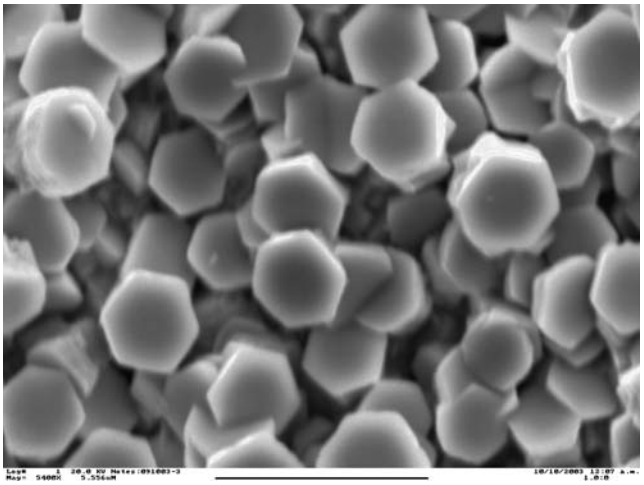

Fig. 4 Morphology of Zn coating deposited from 0.6 M $ZnSO_4$+ 0.5 M Na_2SO_4 solution, pH 1.6 at 300 mA cm^{-2} for 90 s

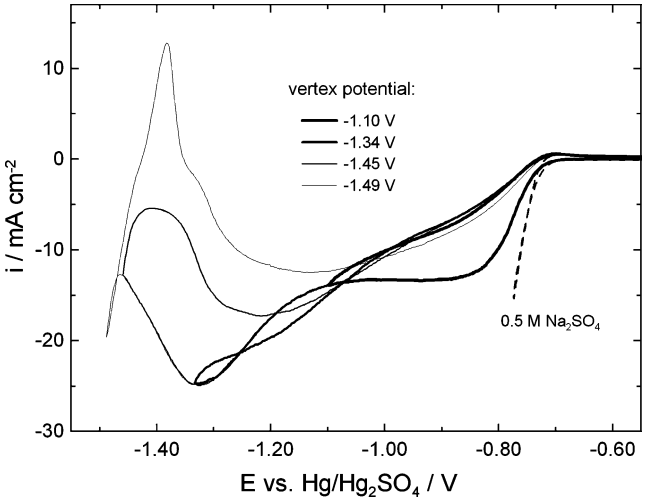

Fig. 6 Voltammograms showing the effect of the polarisation range on the deposition and dissolution of Zn in 0.6 M $ZnSO_4$+0.5 M Na_2SO_4 solution, pH 1.6

potential of about −1.9 V at which co-deposition of Cr is expected to start [30]. However, to avoid/minimise the formation of hydroxo-products of Cr in electrolytes for deposition of Zn–Cr alloy coatings, it was necessary to conduct the electrodeposition process at low pH values. Further investigations were then performed in electrolytes with pH 1.6.

To improve electrolyte conductivity, 0.5 M Na_2SO_4 was added to the 0.6-M $ZnSO_4$ solution (Fig. 3). This electrolyte composition has been used as a base for Zn–Cr alloy deposition [29, 30]. The addition of Na_2SO_4 is reflected in the voltammogram by an increase of the rate of the cathode reaction and a split of the Zn anode maximum as in the case of the voltammogram presented in Fig. 1. A current density of about 300 mA cm^{-2} corresponds to the expected potential of Cr co-deposition (−1.9 V). The morphology of the Zn coating deposited at this current density is presented in Fig. 4. Hexagonal Zn platelets, common for Zn electrodeposits, are observed. For this particular electrolyte, the voltammogram profile up to the region of Zn bulk deposition was studied in more detail.

According to some authors, the UPD shift of Zn(II)–Pt is approximately 1.0 V [19–21] and the process of UPD of Zn occurs simultaneously with hydrogen UPD [7]. The present investigations also evidence the appearance of a cathode and anode maxima in this potential region when the solution contains Zn ions (Fig. 5). At potentials more positive than +0.3 V, formation of an oxide film starts on the Pt electrode, which is then reduced at about −0.1 V during the cathode scan. The cathode maximum at about −0.5 V could be associated with the very initial step of UPD phenomena, i.e. preferential decoration of 0D surface inhomogeneities (point defects, kink sites, etc.) by adsorption of single metal adatoms (0D phase formation) [40].

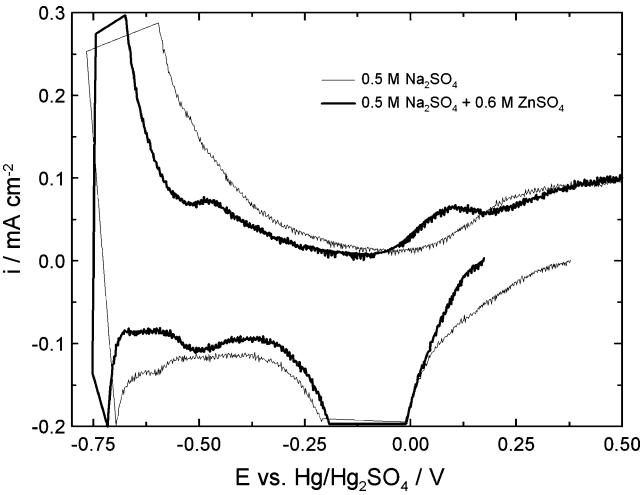

Fig. 5 Voltammograms in 0.5 M Na_2SO_4 and 0.6 M $ZnSO_4$+0.5 M Na_2SO_4 solutions, pH 1.6. Vertex potential −0.8 V

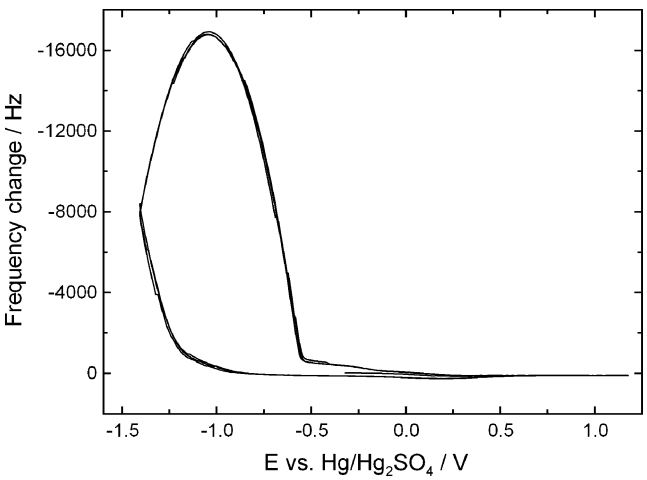

Fig. 7 EQCM ΔF data plotted against the potential; 0.6 M $ZnSO_4$+0.5 M Na_2SO_4 solution, pH 1.6

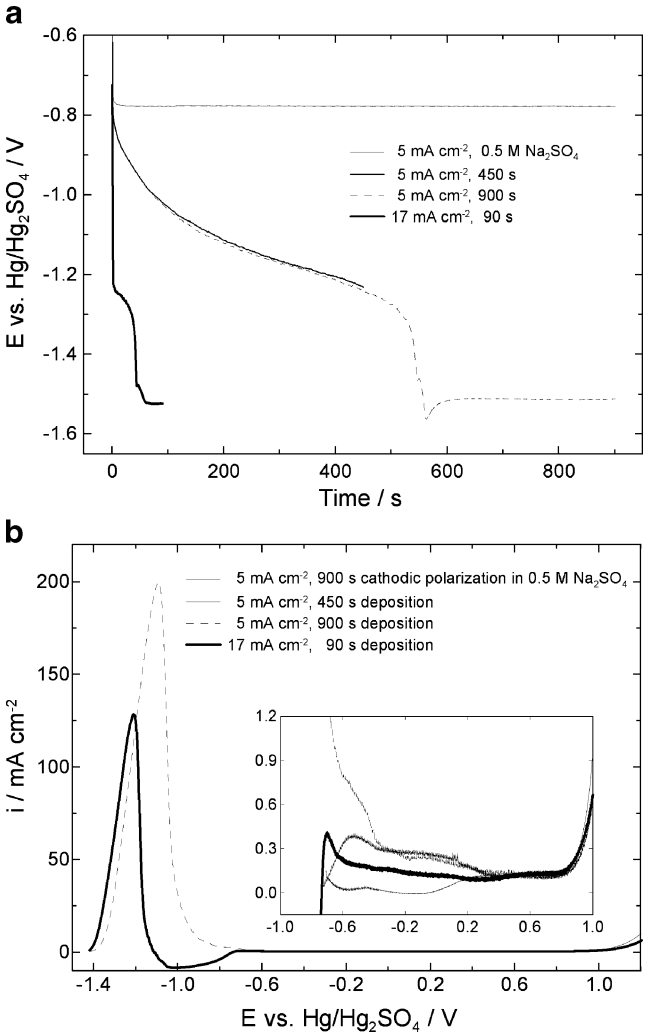

Fig. 8 Galvanostatic potential vs. time curves obtained during Zn deposition in 0.6 M $ZnSO_4$+0.5 M Na_2SO_4 solution, pH 1.6 at different current densities (**a**) and subsequent anodic potentiodynamic curves (**b**). The corresponding curves for 0.5 M Na_2SO_4 solution, pH 1.6 are given for comparison. *Inset* zoom in the potential range −1.0 to +1.0 V

The subsequent increase of the cathode current density, at a potential of about −0.7 V, is due to HER (Figs. 5 and 6). In the presence of Zn ions, the hydrogen reaction is impeded and the limiting current density is considerably lower than that for the Zn-free solution (see also Figs. 1 and 2). A possible explanation of the suppression of the HER could be the evolution of Zn UPD and related phenomena. At potentials of about −1.1 V, the curve "exits" the range of the limiting current for the hydrogen reaction, which is an indication for a further step in the formation of the Zn UPD phase (Fig. 6). Consequently, the rate of the cathode process increases and, at a potential of −1.34 V, a maximum is recorded. It can be seen with the naked eye that evolution of hydrogen declines after the cathode maximum at −1.34 V and stops in the potential region of the minimum at −1.46 V. The decreased rate of the cathode process in the potential region between −1.34 and −1.46 V leads to the assumption that the Zn UPD phase, formed during the forward scan to −1.34 V, is "sufficient" to reduce the contribution of the hydrogen reaction, as a result of the high overvoltage of hydrogen on Zn.

The gravimetric measurements in the potential region of the observed maximum were performed by EQCM. Figure 7 evidences a continuous increase in mass starting from about −0.8 to −1.4 V (the vertex potential) with a significant change in slope ($d\Delta F/dE$) at about −1.1 V. On the reverse scan, the mass increases back to about −1.1 V and then a considerable mass decrease follows at less negative potentials. These results demonstrate that the mass change is reversible and could be attributed to UPD of Zn and dissolution of UPD Zn. The change in mass at potentials more negative than −1.1 V is significant and Δm does not correspond to a Zn overlayer with monatomic thickness. This is an indication for a strong interaction between Zn adatoms and Pt substrate leading to the formation of a 2D phase comprising more than a monolayer. This 2D phase formation could be considered as an initial step of the Zn electrocrystallisation [25, 40, 41]. In the potential range, near the equilibrium for Zn(II)/Zn(0), the Zn deposition is considered to follow the Stranski–Krastanov growth, which predicts the nucleation and growth of 3D clusters on top of the 2D phase. Results from potentiostatic studies in the UPD region, particularly at −1.12 V vs. SCE, show a multilayer growth comparable with the AFM analysis [25]. Of course, the simultaneous hydrogen formation and evolution should be taken into account as well.

After scanning to a vertex potential of −1.34 V (Fig. 6), the loop of the voltammogram is assigned to UPD phase formation and dissolution. Note that, besides UPD, a strong

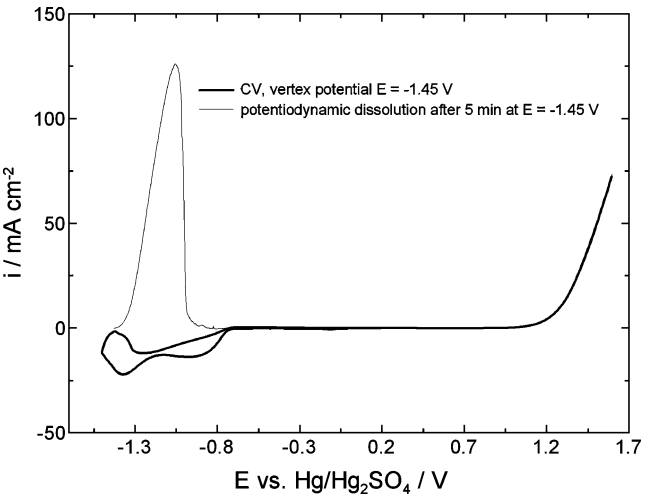

Fig. 9 Voltammogram (vertex potential of −1.45 V) and potentiodynamic curve of Zn dissolution after potentiostatic deposition at −1.45 V in 0.6 M $ZnSO_4$+0.5 M Na_2SO_4 solution, pH 1.6 for 300 s

interaction is also established between the depositing Zn and various substrates (e.g. Pt [18, 21], Au [18, 22], Cu [22]), which results in the formation of alloys. The anode maximum, at about +0.1 V, observed on Fig. 5 could be assigned to the dissolution of such an alloy. Indirect evidence of the occurrence of such a process under the conditions of the present experiments is also provided by the course of the potential–time curves at low current densities, under extended polarisation (Fig. 8a) and the subsequent potentiodynamic dissolution curves (Fig. 8b). At a current density of 5 mA cm^{-2}, corresponding to about −0.76 V on the voltammogram, only a reaction of hydrogen evolution should proceed (Fig. 6). The above potential is reached very quickly after the current is switched on, similar to the polarisation curve in 0.5 M Na_2SO_4 at this current density. But then involvement of other reactions, such as adsorption/desorption of Zn ions, stepwise UPD of Zn and alloy formation, strongly impede the reaction of hydrogen evolution and hence the potential shifts to the region of Zn bulk deposition (Fig. 8a). The subsequent anodic potentiodynamic curve indicates that Zn dissolution starts at the equilibrium potential for Zn electrode for this particular electrolyte (Fig. 8b). After 450 s of electrodeposition, a time insufficient for onset of bulk deposition of Zn, a broad multicomponent maximum is registered in the potential region from −0.7 to +0.3 V, which implies the dissolution of Zn atoms with different atomic surroundings and interaction forces. The curve profile suggests that, in this potential region, the dissolution of UPD Zn and of Zn from the Zn–Pt alloy proceeds. It is difficult to clearly distinguish the initial stages of Zn deposition (UPD) and alloy formation with the Pt substrate, but the binding energy of Zn phase–substrate is weaker than that in a Zn–substrate alloy phase and the dissolution of the alloy phase appears at more positive potentials. After the dissolution of the Zn layer deposited at 17 mA cm^{-2} for 90 s, the potential of the Pt electrode remains in the cathode region of potentials for the HER. The subsequent anodic part of the curve features a maximum at about −0.7 V, most probably due to oxidation of the adsorbed/absorbed hydrogen. Dissolution of the Zn resulting from UPD and from an alloy with Pt is not so clearly pronounced in the curve because of the short time of electrodeposition [21]. The data from the EDX analyses of samples deposited at low current density, 5 mA cm^{-2}, for 700 s and potentiostatically at −1.34 V for 900 s show the presence of Zn in amounts of about 0.3–0.4 mass%.

On scanning to a vertex potential of −1.45 V, no anodic maximum of Zn dissolution is registered (Figs. 6 and 9) because of the short time of polarisation, whilst on potentiodynamic dissolution after potentiostatic deposition at this potential for 300 s, the anodic maximum is clearly manifested (Fig. 9).

From the semi-logarithmic representation of the voltammograms, an equilibrium potential of −1.43 V is determined for the Zn reaction, corresponding to the given Zn(II) concentration (inset in Fig. 3). The same potential value has also been established for samples left in the electrolyte after galvanostatic Zn bulk deposition. The steep rise of the current after the minimum at −1.46 V (Fig. 6) corresponds to the Zn bulk deposition (OPD range) and, at more negative potentials, evolution of hydrogen from water starts as well.

At low current densities, Zn is deposited most probably from the simple hydrated Zn(II) ions, but at high current densities, respectively, potentials more negative than −1.7 V, when alkalisation is sufficiently high, it can be assumed that Zn electroreduction occurs mostly through $ZnOH^+$ ions so that hydroxy-products of Zn are formed and incorporated into the coating. Consequently, the Cr co-deposition with Zn will take place in complex conditions in the vicinity of the electrode.

Conclusions

A decrease of Zn electrolyte pH, so as to minimise/avoid the formation of hydroxo-products of Cr in the electrolyte for deposition of Zn–Cr alloy coatings, leads to a decrease in current efficiency for the Zn reaction and to a significant increase of the current density for reaching the presumed potential of co-deposition of Cr (−1.9 V vs. Hg/Hg_2SO_4). An equilibrium potential of −1.43 V has been determined for the Zn reaction, corresponding to the given Zn(II) concentration. Obviously, a significant proximity of the deposition potentials of Zn and Cr is necessary to deposit a Zn–Cr alloy. The results of the electrochemical investigations in acid Zn electrolytes indicate that Zn bulk deposition is preceded by hydrogen evolution, stepwise Zn UPD and formation of a Zn–Pt alloy. Hydrogen evolution from H_2O starts in the potential range of Zn bulk deposition.

Acknowledgement The investigations have been performed with the support of BMVIT, respectively, FFG and Land Niederösterreich.

References

1. Akiyama T, Fukushima H (1992) ISIJ Int 32:787
2. Aramata A, Taguchi S, Fukuda T, Nakamura M, Horanyi G (1998) Electrochim Acta 44:999
3. Igarashi K, Aramata A, Taguchi S (2001) Electrochim Acta 46:1773
4. Lee JY, Kim JW, Lee MK, Shin H, Shin HJ, Kim HT, Park SM (2004) JECS 151:C25
5. Alvarez A, Salinas D (2004) J Electroanal Chem 566:393
6. Diaz-Arista P, Meas Y, Ortega R, Trejo G (2005) J Appl Electrochem 35:217

7. Mendez PF, Lopez JR, Meas Y, Ortega R, Saldago L, Trejo G (2005) Electrochim Acta 50:2815
8. Ohba M, Panossian Z, Camargo P (2006) Trans Inst Met Finish 84:320
9. Martyak N (2006) J Appl Surf Finish 1:147
10. Roventi G, Bellezze T, Fratesi R (2006) Electrochim Acta 51:2691
11. Gomes A, da Silva Pereira MI (2006) Electrochim Acta 51:1342
12. Gomes A, da Silva Pereira MI (2006) Electrochim Acta 52:863
13. Ballesteros J, Diaz-Arista P, Meas Y, Ortega R, Trejo G (2007) Electrochim Acta 52:3686
14. Lodhi ZF, Mol JMC, Hamer WJ, Terryn HA, De Wit JHW (2007) Electrochim Acta 52:5444
15. Manzoli A, Santos M, Machado S (2007) Thin Solid Films 515:6860
16. Ravindran V, Muralidharan V (2007) Trans Inst Met Finish 85:153
17. Sylla D, Creus J, Savall C, Roggy O, Gadouleau M, Refait Ph (2003) Thin Solid Films 424:171
18. Despic AR, Pavlovic MG (1982) Electrochim Acta 27:1539
19. Quaiyyum MA, Aramata A, Moniwa Sh, Taguchi S, Enyo M (1994) J Electroanal Chem 373:61
20. Taguchi S, Aramata A, Quaiyyum MA, Enyo M (1994) J Electroanal Chem 374:275
21. Guerra E, Kelsall GH, Bastetti M, Dreisinger D, Wong K, Mitchell KAR, Bizzotto D (2004) J Electrochem Soc 151:E1
22. Chu MG, McBreen J, Adzic G (1981) J Electrochem Soc 128:2281
23. Rashkov S, Bozhkov C, Kudryavtsev V, Pedan K, Bagaev S (1988) J Electroanal Chem 248:421
24. Nicol MJ, Philip HI (1976) J Electroanal Chem 70:233
25. Gomes A, Viana A, Pereira S (2007) J Electrochem Soc 154:D452
26. Sudha V, Sangaranarayanan MV (2005) J Chem Sci 117:207
27. Song KD, Kim KB, Han SH, Lee H (2004) Electrochem Solid-State Lett 7:C20
28. Popov BN, Zheng G, White RE (1994) Corr Sci 36:2139
29. Boiadjieva Tz, Monev M, Raichevski G (2001) UPB Sci Bull Series B 63:135
30. Boiadjieva Tz, Kovacheva D, Petrov K, Hardcastle S, Sklyarov A, Monev M (2004) J Appl Electrochem 34:315
31. Boiadjieva Tz, Kovacheva D, Petrov K, Hardcastle S, Monev M (2004) Corr Sci 46:681
32. Boiadjieva Tz, Petrov K, Raichevski G, Monev M (2006) Trans Inst Met Finish 84:313
33. Pourbaix M (1966) Atlas of electrochemical equilibria in aqueous solutions. Pergamon, London
34. Ohgai T, Ki J, Akiyama T, Fukushima H (1998) In: Value-Addition Metallurgy, Edited by W.D. Cho and H.Y. Sohn, The Minerals, Metals & Materials Society 225
35. Akiyama T, Kobayashi S, Ki J, Ohgai T, Fukushima H (2000) J Appl Electrochem 30:817
36. Watson A, Su YJ, el-Sharif MR, Chisholm CU (1993) Trans Inst Met Finish 71:15
37. Takahashi A, Miyoshi Y, Hada T (1994) J Electrochem Soc 141:954
38. Howarth JN, Pletcher D (1988) J Appl Electrochem 18:644
39. Horeva NK, Suhotin AM (1982) Elektrohimija 18:20
40. Budevski E, Staikov G, Lorenz WJ (1996) Electrochemical phase formation and growth. VCH, Weinheim
41. Vasilakopoulos D, Bouroushian M, Spyrellis N (2007) In: International Conference EUROINTERFINISH, book of abstracts, Athens, 18–19 October